THE ASTROPHYSICAL JOURNAL, 299:416–423, 1985 December 1

EMISSION FEATURES IN THE 4–13 MICRON SPECTRA OF THE REFLECTION NEBULAE NGC 7023 AND NGC 2023

K. SELLGREN[1,2]
Institute for Astronomy, University of Hawaii

AND

L. J. ALLAMANDOLA,[1] J. D. BREGMAN, M. W. WERNER,[1] AND D. H. WOODEN
Space Science Division, NASA Ames Research Center
Received 1985 March 11; accepted 1985 May 30

ABSTRACT

Spectroscopy from 4 to 13 μm of the visual reflection nebulae NGC 7023 and NGC 2023 has been obtained. These data, together with previous work from 1 to 4 μm, show that the spectra of these sources consist of a relatively flat continuum from 1 to 13 μm and six emission features at 3.3, 3.4, 6.2, 7.7, 8.6, and 11.3 μm. The observations rule out equilibrium thermal emission for the features and continuum in reflection nebulae, and point toward a nonequilibrium emission mechanism such as thermal emission from thermally fluctuating small grains or fluorescence from large molecules. The similarity of the emission feature spectra in reflection nebulae to those in other sources suggests a universal emission mechanism, thus implying nonequilibrium emission mechanisms in other sources.

Subject headings: infrared: spectra — nebulae: individual — nebulae: reflection — radiation mechanisms

I. INTRODUCTION

Surprisingly strong near-infrared emission from visual reflection nebulae was found recently by Sellgren, Werner, and Dinerstein (1983, hereafter Paper I) and Sellgren (1984, hereafter Paper II). The 1–5 μm spectra of these sources are characterized by a smooth, flat continuum and strong emission features at 3.3 and 3.4 μm; the emission is much too intense to be due to scattered light. Other mechanisms such as free-free emission, equilibrium thermal emission from dust, background stars, and vibrational fluorescence from simple molecules in grain mantles were also ruled out in Papers I and II. A model was proposed in Paper II to explain the continuum emission—and possibly also the 3.3 and 3.4 μm feature emission—as thermal emission from very small grains, with radii $\sim$10 Å, each of which is briefly heated to temperatures of $\sim$1000 K by the absorption of single ultraviolet photons.

This paper presents spectrophotometric observations of two of the above reflection nebulae, NGC 7023 and NGC 2023, from 5 to 13 μm, made to address the following points. First, by searching for continuum emission at longer wavelengths, these observations could test the predictions of the thermal fluctuation model. Second, the observations were made to search for companion features to the 3.3 μm feature at 6.2, 7.7, 8.6, and 11.3 μm. These are seen in all other sources in which the 3.3 μm feature is seen.

II. OBSERVATIONS

Table 1 summarizes our observations of NGC 7023 and NGC 2023. All observations were made 30″ W 20″ N of HD 200775 in NGC 7023, and 60″ S of HD 37903 in NGC 2023, except for the Kitt Peak 1.3 m observations, where measurements were obtained both 30″ W 20″ N and 30″ N of HD 200775.

The observations at wavelengths longer than 4.8 μm were calibrated using the magnitudes given by G. Neugebauer (private communication) for β And, α Tau, α Ori, α Her, and β Peg. For the 5–8 μm spectrophotometry, a blackbody was fitted through the 4.8 and 10 μm broad-band magnitudes of the standard star, while for the 8–13 μm spectrophotometry we interpolated between the 10 μm narrow-band magnitudes. The 3.7–4.1 μm spectrophotometry was calibrated relative to an A star, HD 162208, by adopting at longer wavelengths the 2.2 μm mag given for this star by Elias *et al.* (1982). The 4.8 μm broad-band measurement was calibrated relative to the O9.5 star ζ^1 Ori by adopting the 3.4 μm mag given by G. Neugebauer (private communication) at 4.8 μm. This measurement at 4.8 μm was averaged with the earlier 4.8 μm observations of Paper I to improve the signal-to-noise ratio. The flux densities for zero magnitude of Beckwith *et al.* (1976) were adopted for all observations. No correction was made for instrumental scattered light from HD 200775 in NGC 7023 or HD 37903 in NGC 2023, as this correction was measured to be 1% or less of the nebular flux density at all wavelengths observed.

The 24 channel grating array spectrometer, described by Witteborn and Bregman (1984), was used on the Kuiper Airborne Observatory with 23 working detectors, with each channel covering one resolution element. The integration time on NGC 7023 was 22 minutes, and 47 minutes on NGC 2023. The typical 1 σ uncertainty for each resolution element was 7×10^{-18} W cm^{-2} μm^{-1} in a 20 minute integration time. Where the resulting signal-to-noise ratio was less than three, adjacent channels were averaged together to produce either a detection or a 3 σ upper limit at the center of the wavelength range covered by the averaged channels.

The uncertainties for the 8–13 μm and 3.7–4.1 μm spectrophotometry are statistical uncertainties determined at each wavelength separately. The calibration uncertainty is 5% for

[1] Visiting Astronomer at the Infrared Telescope Facility, which is operated by the University of Hawaii under contract to the National Aeronautics and Space Administration.

[2] Visiting Astronomer, Kitt Peak National Observatory, operated by the Association of Universities for Research in Astronomy, Inc., under contract with the National Science Foundation.

TABLE 1

OBSERVATIONS

Telescope[a]	λ (μm)	Dates of Observations	R[b]	Beam[c]	Chop Angle[d]	Instrument[e]
		NGC 7023				
KPNO	8–13	1983 Aug 11–12	1.7	27	90	CCCP
IRTF	8–13	1983 Oct 27–28	2.4	11	90	AT-1
IRTF	3.7–4.1	1983 Oct 31	1.7	10	90	RC-2
KAO	5.2–8.0	1983 Nov 30–Dec 1	2.0	21	30	FOGS
		NGC 2023				
IRTF	8–13	1983 Oct 27–28	2.4	11	90	AT-1
KAO	5.2–8.0	1983 Nov 30–Dec 1	2.0	21	108	FOGS
IRTF	8–13	1984 Feb 8–11	2.4	11	90	AT-1
IRTF	4.8[f]	1984 Feb 12	...	11	90	RC-2

[a] Telescopes used were the Kitt Peak National Observatory (KPNO) 1.3 m, the 3.0 m Infrared Telescope Facility (IRTF), and the 0.9 m Kuiper Airborne Observatory (KAO).

[b] Spectral resolution (R), in percent, of spectrophotometry.

[c] Diameter (full width half-maximum) of beam in arc seconds.

[d] Chopper position angle in degrees east of north; the throw was 120″ in all cases.

[e] Instruments used were a Si:Ga photoconductor cooled to 10 K by a two-stage Joule-Thomson refrigerator with a circular variable filter wheel (CCCP), a LHe-cooled Si:As photoconductor with a circular variable filter wheel (AT-1), a solid nitrogen-cooled InSb detector with a circular variable filter wheel (RC-2), and a LHe-cooled grating array spectrometer with 24 Si:Bi photoconductor detectors (FOGS).

[f] 4.8 refers to a single broad-band measurement.

the 3.7–4.1 μm spectrophotometry and 15% for all other observations.

All observations were converted to surface brightnesses, after correcting for the difference in sensitivity between a point source and a uniformly extended source, using scans of point sources. The assumption of uniform surface brightness in comparing observations obtained with different beam sizes is justified by the good agreement of the surface brightnesses measured at 2.2 μm with 5″, 10″, and 30″ beams in NGC 7023; at 2.2 μm with 10″, 30″, and 60″ beams in NGC 2023; and at 11.3 μm with 11″ and 27″ beams at one position in NGC 7023 (Papers I, II, and this paper.)

III. RESULTS

Figure 1 shows the spectra from 1 to 13 μm of the reflection nebulae NGC 7023 and NGC 2023. The spectrophotometry at wavelengths longer than 3.7 μm is from the observations described in this paper. The shorter wavelength spectrophotometry and 1.25–4.8 μm photometry is from Papers I and II, except for the 4.8 μm photometry of NGC 2023, which is an average of data from this paper and Paper I.

The spectra in Figure 1 are characterized by the six well-known emission features at 3.3, 3.4, 6.2, 7.7, 8.6, and 11.3 μm, generally known as the unidentified infrared emission features. These features have been seen in many other sources, such as H II regions, planetary nebulae, and galaxies, with relative values of the feature intensities, corrected for continuum, which are similar to those seen in Figure 1 (see Aitken 1981). Note that while the wavelength coverage from 8 to 13 μm is limited, the strong 11.3 μm feature in these two sources is defined by detections of, or upper limits to, the continuum levels on either side of the feature. Our upper limit at 10 μm in NGC 2023 also rules out the presence of silicate emission at 10 μm in this reflection nebula. The spectra of the two reflection nebulae are rather similar, particularly in the overall shape of the continuum and the strength of the features relative to the continuum. The spectral shapes of the 6.2 and 7.7 μm features are also the same, within the errors, in the two nebulae. There are, however, some variations in the strengths of the features relative to each other. The ratio of flux density in the 6.2 or 7.7 μm features, to the flux density in the 3.3 μm feature, is about a factor of 2 higher in NGC 7023 than in NGC 2023. The ratio of 11.3 to 3.3 μm flux densities is, however, about the same at the two nebular positions shown in Figure 1. A 3 σ upper limit to the 11.3 μm surface brightness 30″ N of HD 200775 in NGC 7023, less than 2.3×10^{-9} W cm^{-2} μm^{-1} sr^{-1}, is consistent with the ratio of 11.3 to 3.3 μm flux densities observed at the two nebular positions shown in Figure 1.

It is difficult to define the continuum level from 1 to 13 μm in the spectra of NGC 7023 and NGC 2023, due to the increasing dominance of the emission features at longer wavelengths, but it appears to be relatively flat and broader than a single-temperature blackbody. The 4.8 μm broad-band point appears to fall at a minimum in the 1–13 μm continuum, while the "continuum" level between the 6.2 and 7.7 μm features is higher than either the 1–4 or 9–13 μm continuum levels, particularly in NGC 7023.

Table 2 presents the surface brightnesses of the six unidentified emission features in NGC 7023 and NGC 2023. The adopted "continuum" surface brightness is also given. The "continuum" surface brightness was determined by spectral points adjacent to the features, which underestimates the feature flux, particularly for the 6.2 and 7.7 μm features. We adopted these conservative "continuum" points to be consistent with the definitions of previous investigators, and note the true continuum for the 6–9 μm region is probably at the same low level as the 3 and 11 μm continua. The feature-to-continuum ratios are given, along with α_{ph}, the fluorescence efficiency required for the conversion of UV photons to feature photons if the features are to be explained by fluorescence (Dwek *et al.* 1980). The values of α_{ph} were calculated from the feature emission integrated over the spatial extent of the

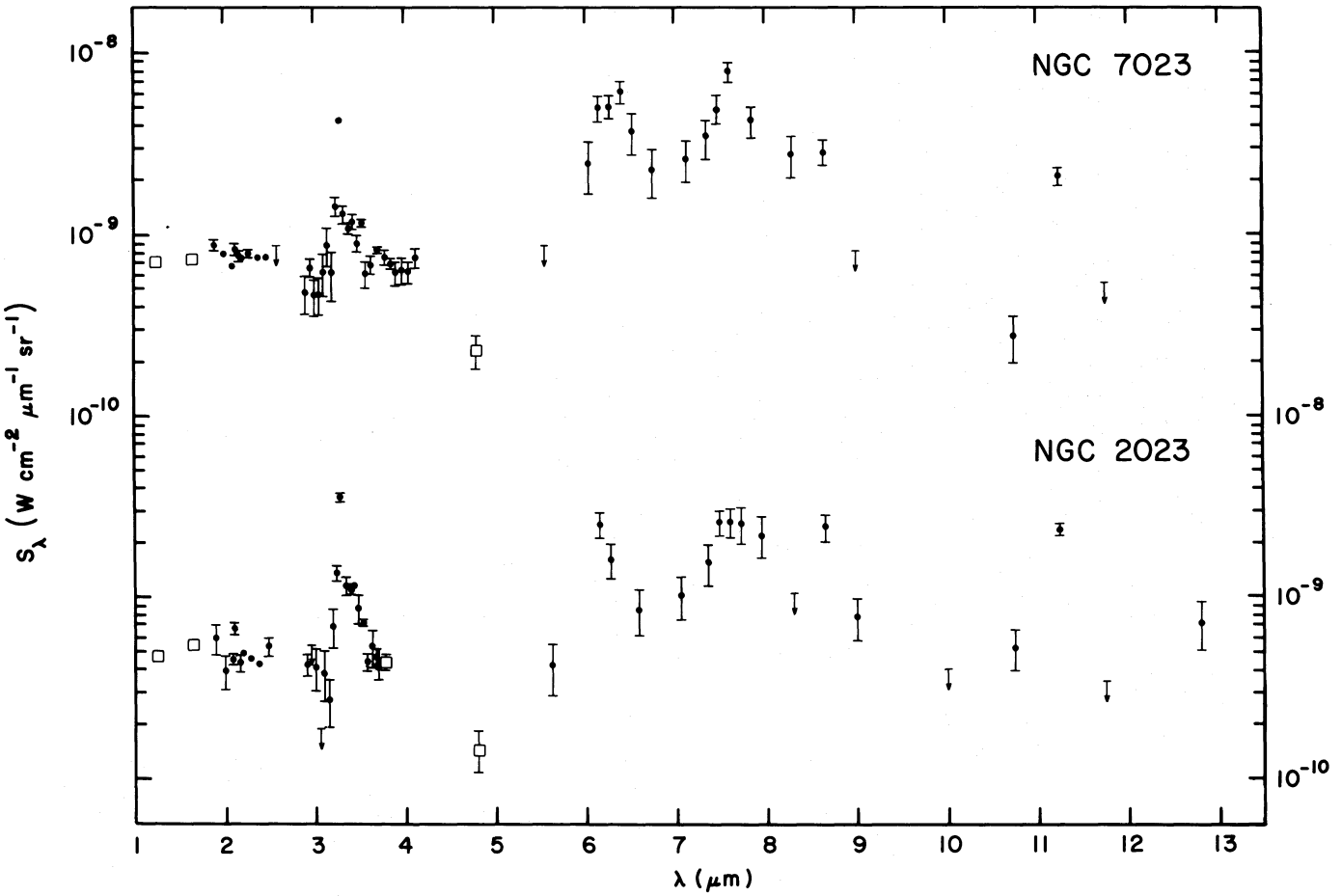

FIG. 1.—Near-infrared spectra of positions in NGC 7023 (*top*) and NGC 2023 (*bottom*). Positions observed are 30″ W 20″ N of HD 200775 in NGC 7023, and 60″ S of HD 37903 in NGC 2023. Filled circles are spectrophotometry with 1%–2% resolution; spectrophotometry at wavelengths longer than 3.7 μm is from this paper, while data at shorter wavelengths are from Papers I and II. Open squares are broad-band photometric measurements from Papers I and II. The 4.8 μm broad-band photometry of NGC 2023 (*bottom*) is an average of data from this paper and Paper I. Error bars represent ±1 σ uncertainties, and are only shown when larger than ±5%. Upper limits are 3 σ upper limits on the spectrophotometry. Spectrophotometry from 5.20 to 7.96 μm was sampled every 0.12 μm; where the signal-to-noise ratio was less than 3, adjacent channels were averaged together to produce detections or upper limits at the center of the wavelength range covered by averaged channels.

nebulae, as described below. The value of α_{ph} summed over all features is ~1 in NGC 7023 and ~3 in NGC 2023.

The similarity of the 1–13 μm spectra of these two nebulae and the constancy of the 1–4 μm spectra at several nebular positions (Paper I) suggest that the integrated luminosity in the near-infrared of these nebulae can be derived by assuming that the 1–13 μm emission spectrum is the same throughout the nebulae. With this assumption, the surface brightness at the nebular positions observed can be scaled by the ratio of the integrated 2.2 μm nebular flux density to the 2.2 μm surface brightness (Paper II) to obtain the integrated luminosity. This implies that the six unidentified features contribute 35 and 130 $L_\odot$ in NGC 7023 and NGC 2023, respectively, to the nebular luminosity. This luminosity in the features is ~1%–2% of the central star luminosity. Integrating over the entire near-infrared spectrum of NGC 7023 implies that the features contribute about one-third of the 1–13 μm nebular flux, with the remainder in the continuum. The fraction of the nebular flux due to the features will be larger if less conservative values for the "continuum" near 6.2 and 7.7 μm are chosen.

Both NGC 7023 and NGC 2023 were detected at 11 μm by the CRL survey (Price and Walker 1976) at a level far in excess of the emission expected from the cold (40–60 K) dust seen in the far-infrared by Whitcomb *et al.* (1981) and Harvey, Thronson, and Gatley (1980). Neither of the central stars of the reflection nebulae are bright enough to contribute significantly to the total 11 μm flux densities observed. We integrated the spectra shown in Figure 1 over the bandpass of the 11 μm filter of the CRL survey, treating upper limits as detections, as they are similar in level to the continuum detections, and scaled again as above. This yields 11 μm nebular flux densities that are 30% and 80% of the observed CRL 11 μm flux densities for NGC 7023 and 2023, respectively. This is in fair agreement, considering the difficulty of properly scaling a measurement made with an 11″ beam to the 3.4 × 10.5 beam of the CRL survey.

The nebular peaks of both NGC 7023 and NGC 2023 appear as sources in the *IRAS* Point Source Catalog. The *IRAS* field of view at 12 μm is 0.76 × 4.5; the nebular peak, however, must have an effective size less than or on the order of 0.76 to have satisfied the point source criteria. Our surface brightnesses integrated over the *IRAS* passband agree to 15% with the 12 μm point source flux densities, if one adopts a source size of 0.76. This agreement in NGC 7023 depends on the assumption that both the central star, which produces 27% of the *IRAS* 12 μm flux density, and the nebular peak are

TABLE 2

UNIDENTIFIED EMISSION FEATURES IN REFLECTION NEBULAE

λ[a] (μm)	S_λ (feature)[b] (10^{-9} W cm^{-2} μm^{-1} sr^{-1})	S_λ ("continuum")[c] (10^{-9} W cm^{-2} μm^{-1} sr^{-1})	Feature-to-Continuum Ratio[d]	α_{ph}[e]
NGC 7023:30″ W 20″ N				
3.3.....	4.2	0.6	5.6	0.02
3.4.....	1.2 ± 0.1	0.6	0.8	0.003
6.2.....	5.0 ± 0.7	2.3	1.2	0.12
7.7.....	7.9 ± 1.0	2.3	2.5	0.77
8.6.....	2.8 ± 0.5	1.5	0.9	0.13
11.3.....	2.1 ± 0.3	0.4	4.4	0.20
NGC 2023:60″ S				
3.3.....	3.6 ± 0.1	0.4	7.4	0.08
3.4.....	1.2	0.4	1.7	0.02
6.2.....	2.5 ± 0.4	0.8	2.0	0.32
7.7.....	2.6 ± 0.5	0.8	2.0	1.0
8.6.....	2.4 ± 0.4	0.9	1.7	0.61
11.3.....	2.4 ± 0.2	0.4	4.6	1.0

[a] Wavelength of feature in microns.

[b] Surface brightness in feature, with no correction for continuum. Uncertainties are 1 σ statistical uncertainties, given only when larger than 5%.

[c] Adopted surface brightness in the "continuum" near the feature. This "continuum" level was derived for convenience from the spectral points nearest each feature, and does not necessarily reflect the true continuum level. No statistical uncertainties are given, since the dominant uncertainty is in the choice of a continuum level, particularly at the longer wavelengths.

[d] Ratio of surface brightness at the peak of the feature, corrected for "continuum," to "continuum" surface brightness.

[e] Fluorescence efficiency, or ratio of the number of feature photons to the number of ultraviolet photons absorbed by dust, as defined by Dwek *et al.* 1980.

included in the point source measurement, an assumption consistent with the *IRAS*-pointing uncertainties. The central star of NGC 2023 contributes negligibly to the 12 μm flux density of that source. A more detailed comparison of ground-based and *IRAS* measurements in reflection nebulae will require use of the *IRAS* all-sky images.

IV. THE EMISSION MECHANISM

The present observations of the unidentified emission features in reflection nebulae can contribute significantly to our understanding of the nature of the emission mechanism. The reflection nebula observations rule out the equilibrium thermal emission model proposed by Dwek *et al.* (1980) for the emission features, since the brightness temperature of the 3.3 μm emission in these sources (190 K) is higher than the maximum temperature (70–150 K) of a dust grain in radiative equilibrium with the central stars of the nebulae (Paper I). An alternate model, attributing the feature emission to ultraviolet-induced vibrational fluorescence from molecules in grain mantles, has been proposed by Allamandola, Greenberg, and Norman (1979). The high value of α_{ph} in the reflection nebulae, however, is difficult to achieve in the vibrational fluorescence model proposed by Allamandola, Greenberg, and Norman. The required fluorescence efficiency is even higher if a common emission mechanism is adopted for the continuum and the features, which may be appropriate considering the constancy of the feature-to-continuum ratios in different reflection nebulae and at different positions in individual reflection nebulae (this paper and Paper I).

In view of the inability of these earlier theories to account for the present observations, we feel that it is more fruitful to search for an explanation of the features and the apparently associated continuum along one or more of the paths outlined below.

a) *Thermal Fluctuations in Small Grains*

In Paper II a model for explaining the 1–5 μm continuum emission was proposed, involving thermal emission from very small grains of radius $\sim$10 Å briefly heated to high temperatures by the absorption of a single UV photon. This model successfully predicts the fraction of the nebular luminosity, $\sim 10^{-2}$, involved in the 1–5 μm near-infrared emission, and requires only a small fraction, $\sim 10^{-3}$, of the total mass of grains to be in the form of $\sim$10 Å sized grains. This type of model may apply to the emission features as well as to the continuum.

The thermal fluctuation model was fit in Paper II to the 1–5 μm continuum, which can be roughly characterized by a gray body of $\sim$1000 K. The observations of this paper show that a single-temperature blackbody is too narrow and provides a poor fit to the 1–13 μm continuum observations. If the nebular flux is due to thermal emission, then clearly a range of grain temperatures must be required. One test of the model is thus whether it can reproduce the observed shape of the continuum emission from 1 to 13 μm. In the Appendix, the predicted surface brightness as a function of wavelength is integrated over a range of grain temperatures determined both by the grain size distribution and by the time dependence of the temperature as an individual grain cools. The results of this calculation are compared with the observations shown in Figure 2. The shape of the predicted flux distribution with wavelength can be fit well to the continuum observations in the reflection nebulae. At the shortest wavelengths, 1–2 μm, the predicted flux begins to fall below the observed spectrum. This is in qualitative agreement with the polarization observations of

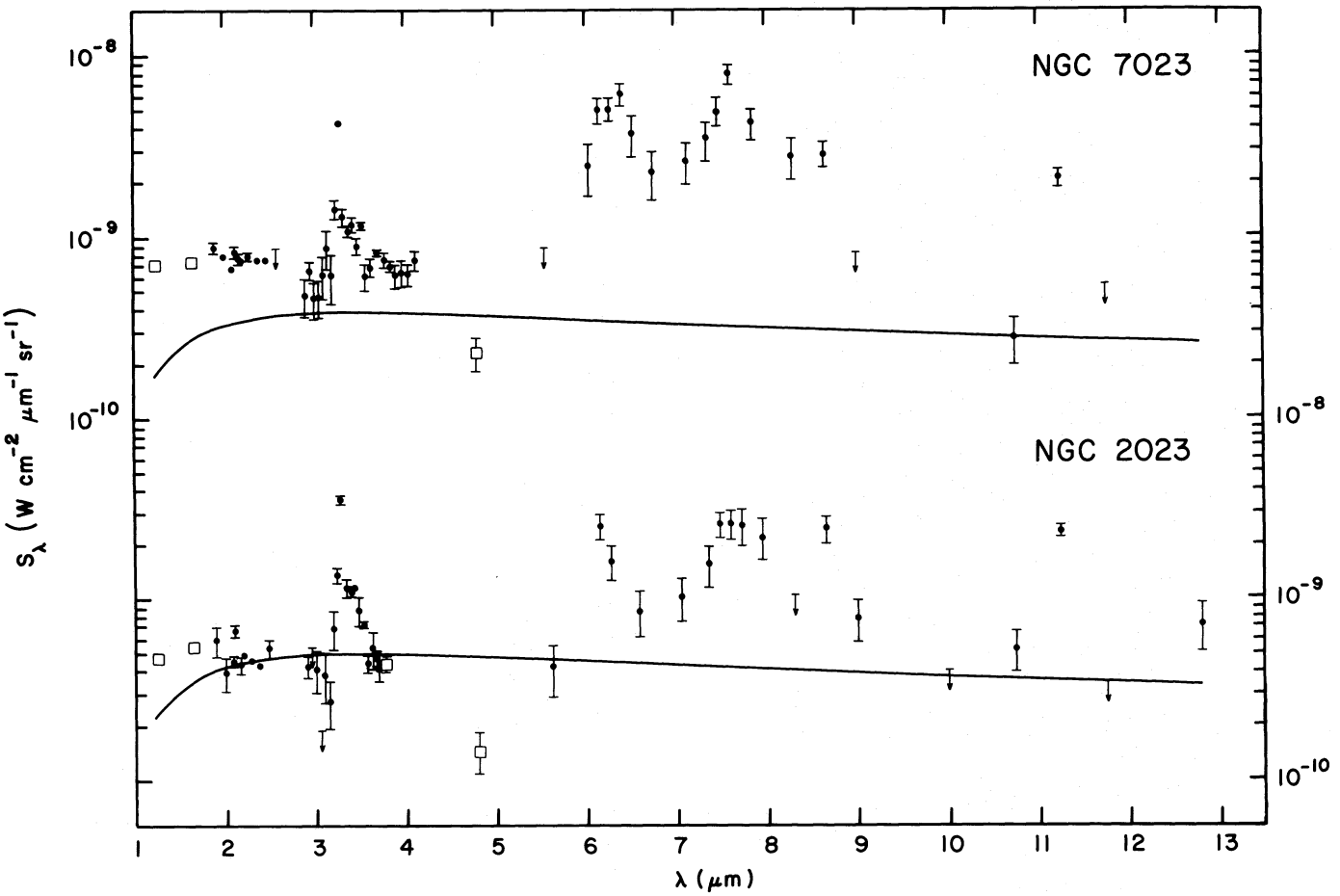

FIG. 2.—Near-infrared spectra of NGC 7023 and NGC 2023, from Fig. 1, compared with continuum energy distribution (*solid curve*) predicted by thermal fluctuation model, as described in the Appendix. Solid curve was normalized to the observations at 10.75 μm in NGC 7023 and to upper limit at 11.74 μm in NGC 2023.

NGC 7023, which show that the fraction of the near-infrared emission due to reflected light is small at 2.2 μm, but becomes increasingly important as the wavelength decreases to 1.25 μm (Sellgren, Werner, and Dinerstein 1985).

Comparisons with the more sophisticated thermal fluctuation calculations of Draine and Anderson (1985) give results similar to our more approximate methods and show reasonable agreement with the 1–13 μm continuum observed in NGC 7023 and NGC 2023. Their graphite spectrum was chosen for comparison, as there is no evidence for silicate emission in either reflection nebula. The predictions of Draine and Anderson fall too short of the observed continuum in the 1–3 μm region, although they provide a good fit at longer wavelengths. This is probably due to their adoption of an effective temperature for the radiation field that is cooler than that of the central stars of NGC 7023 and NGC 2023, and possibly also due to adopting too large a value for the minimum particle size.

b) Nonequilibrium Emission from Large Molecules

Leger and Puget (1984) have proposed that the feature emission is due to nonequilibrium thermal emission from large aromatic molecules, in the gas phase, excited by ultraviolet photons. Using a thermal model, they calculated the emission spectrum of the polycyclic aromatic hydrocarbon (PAH) coronene, and found good spectroscopic agreement with the features. In their paper Leger and Puget do not account for the continuum emission observed in reflection nebulae, since they argue that only lines should be emitted. In a subsequent paper (Puget, Leger, and Boulanger 1985) they derive continuum emission from 1 to 3 μm from electronic transitions, and argue that longer wavelength continuum emission may be due to a superposition of weaker lines.

Allamandola, Tielens, and Barker (1985*a*) argue that it is incorrect to treat emission from PAHs as a thermal phenomenon. Using the single-photon excitation process suggested in Paper II, they calculate the emission spectrum expected from one PAH, chrysene, and again found spectroscopic agreement with the features. In this picture, the continuum could be produced in two ways, either by emission from the lowest lying electronic states, or by emission from the vibrational quasi-continuum (e.g., the low-lying continuum produced by the overlap of all the various overtone and combination bands). At present, this theory shows promise for understanding the emission features, but does not make any predictions as to the shape of the continuum. It can be distinguished from the Leger and Puget model by detailed analysis of the intensity ratios of the various infrared features, as discussed by Allamandola, Tielens, and Barker (1985*b*). These gas-phase fluorescent mechanisms offer more promise than the original suggestion of fluorescence of molecules in grain mantles because, in the

former case, there are no nonradiative mechanisms competing for the de-excitation of the molecules.

V. IMPLICATIONS

The reflection nebula observations have important implications for the general nature of the feature-emitting dust. The features seen in reflection nebulae are the same as are seen in H II regions, planetary nebulae, bipolar nebulae, and galaxies. The similarity of the feature flux ratios in all these sources argues strongly for a universal emission mechanism. The energetics of grain heating in reflection nebulae points to a nonequilibrium process, such as thermal emission from thermally fluctuating grains, or fluorescence from large molecules. The spatial distribution of the feature and continuum emission in reflection nebulae (Papers I and II) shows that both are proportional to the visual or UV radiation incident on the emitting grains.

Visual reflection nebulae such as NGC 7023 and NGC 2023 provide an ideal opportunity to study the emission characteristics of feature emitting "dust." The continuum emission that is observed in reflection nebulae appears to be associated with the features, as suggested by the constancy of the feature-to-continuum ratios. The absence of competing sources of continuum emission can be readily understood. Due to the late spectral type of the illuminating star of a reflection nebula, there is little or no ionized gas within the nebula. This, in turn, means that there is no trapped Lyα radiation to heat dust within an H II region to high enough equilibrium temperatures to emit significantly in the near-infrared. Furthermore, the lack of a significant H II region implies that the observed near-infrared spectrum of a reflection nebula will not contain contributions from other emission mechanisms such as free-free radiation or atomic line emission. Direct starlight is also insufficient to heat dust to equilibrium temperatures capable of contributing significantly to the near-infrared emission. Reflected light may contribute some to the near-infrared nebular emission, but its amount can be estimated from polarization measurements or from the ratio of nebular surface brightness to central star flux density. Thus, except for a small reflected light component, most prominent at the shortest wavelengths (Sellgren, Werner, and Dinerstein 1985), the near-infrared spectrum of a reflection nebula probably represents the pure emission spectrum of the dust that is associated with the unidentified emission features.

The ubiquitous nature of the unidentified infrared emission features and the fact that the "dust" that emits them does not appear to require any special processing imply that to understand interstellar grains at all one must understand the feature-emitting grains. The quiet environment of the reflection nebulae implies that the emission is easily excited and does not require the presence of ionized gas, ionization fronts, shocks, or high-luminosity sources. The feature-emitting dust can exist, and the features be formed, over a range of UV illumination, as the illumination levels at the Orion ridge are ~ 10 times higher than in the reflection nebulae. The feature-emitting dust is easily made, as the presence of the features in the newly formed dust surrounding planetary nebulae shows. The dust is either difficult to alter or destroy, or is easily replenished, since the same features are seen in the young dust in planetaries and in the old dust associated with reflection nebulae, which has survived processing in the interstellar medium as well as the collapse of a molecular cloug and an epoch of star formation.

One implication of the ubiquitous and sturdy nature of the feature-emitting material is that one might expect to see low surface brightness diffuse emission from the features associated with the general galactic background. To date, the two common characteristics of feature-emitting regions are the presence of dust and ultraviolet radiation, both of which are present in the general interstellar medium. In light of this possibility, it is interesting that Phillips, Aitken, and Roche (1984) have found, in their study of the 8–13 μm spectra of galaxies with H II region nuclei, that the 8–13 μm spectra of these galaxies are atypical of galactic H II regions, showing little emission from silicate grains, and have feature-to-continuum ratios for the 8.6 and 11.3 μm features intermediate between values typical of a galactic H II region and of a reflection nebula. Phillips *et al.* attributed this to observing more of the material on the edge and outside H II regions in external galaxies than is seen when observing galactic H II regions, since the feature-to-continuum ratios in galactic H II regions are lowest in the center, and increase toward the edges of the H II regions (Sellgren 1981). An alternate explanation suggested by the present results is that the 8.6 and 11.3 μm feature emission from galaxies is enhanced by emission from diffuse UV-illuminated dust not associated with H II regions. Distinguishing between these explanations for the 8–13 μm observations of galaxies would have interesting consequences for the near-infrared galactic background.

The observations of the unidentified near-infrared emission features, and of the near-infrared continuum emission in reflection nebulae, have made clear the necessity for much supporting laboratory and theoretical work. Laboratory and theoretical investigations of small grains and/or large molecules are required to determine whether continuum emission like that observed in reflection nebulae can be produced and whether the details of line emission from such particles match those of the unidentified emission features. Finally, the question of whether very small grains can be made and can survive needs further theoretical consideration.

VI. CONCLUSIONS

This paper presents 1–13 μm spectrophotometry of the visual reflection nebulae NGC 7023 and NGC 2023. The spectra are dominated by the unidentified infrared emission features, which are much too strong to be produced by scattering. A flat continuum from 1 to 13 μm is also present; the feature-to-continuum ratios for the 3.3 and 11.3 μm features are ~ 5–7. The relative strengths and shapes of the features are identical to those seen in other sources. No evidence is seen for 10 μm silicate emission.

Because of the absence of other near-infrared emission mechanisms and the relative quiescence of the environment, it is clear that reflection nebulae are the ideal sites for the study of the near-infrared features and the apparently associated continuum. The principal conclusions of this initial work are the following.

1. The observations rule out equilibrium thermal emission for the source of the features and point to a nonequilibrium emission process such as fluorescence from large molecules or thermal emission from thermally fluctuating small grains. Predictions of a thermal fluctuation model fit the continuum seen in reflection nebulae and may also explain the feature emission.

2. The similarity of the relative feature strengths in reflection nebulae to those seen in other feature-emitting sources argues

that the same nonequilibrium emission mechanism operates in all sources showing these features.

3. The quiescent environment of reflection nebulae implies that the features are associated with the interstellar medium, rather than with a particular source of excitation. The feature-emitting material must be hardy, ubiquitous, and easily produced.

4. The unidentified emission features apparently dominate the near-infrared spectrum of ordinary interstellar material illuminated by ultraviolet radiation. This fact may have important implications for the diffuse near-infrared emission from our own and other galaxies. Understanding the emission mechanism and material for the unidentified infrared emission features is critical to understanding the near-infrared emission of the interstellar medium, and by extension, to understanding the nature of interstellar matter.

We would like to thank the staff of the Kuiper Airborne Observatory and the members of the Medium Altitude Missions Branch at Ames Research Center for their contributions to the success of our flight series. We also thank R. W. Capps, W. Golisch, D. Griep, C. Kaminski, Y. Pendleton, and A. Tielens for assistance with the observations; L. Craven, R. Joyce, K. M. Merrill, and F. C. Witteborn for assistance with the equipment; and J. Mathis for helpful comments on the manuscript. Valuable discussions were held with E. E. Becklin, H. L. Dinerstein, I. Gatley, A. Leger, B. T. Soifer, F. C. Witteborn, and C. G. Wynn-Williams. One of the authors (K. S.) was at Space Telescope Science Institute when this work was begun.

APPENDIX

SPECTRUM OF NONEQUILIBRIUM THERMAL EMISSION FROM SMALL GRAINS

Thermal emission from thermally fluctuating grains has been previously considered by Duley (1973), Greenberg and Hong (1974), Harwit (1975), Allen and Robinson (1975), Purcell (1976), and Aannestad and Kenyon (1979). All of these authors, however, have considered only the low temperature limit of the heat capacity and thermal fluctuations in cold interstellar grains. In the following, we derive the energy distribution of grains in the high temperature limit of thermal fluctuations, where temperatures are high enough to account for the near-infrared emission we observe in reflection nebulae. We adopt a bulk material approach to the properties of the grains.

The power per unit wavelength P_λ emitted by an individual grain of radius a and temperature T is

$$P_\lambda = \pi B_\lambda(T) 4\pi a^2 Q_\lambda(a) , \tag{A1}$$

where B_λ is the Planck function, λ is the wavelength, and $Q_\lambda(a)$ is the grain emissivity. For convenience $Q_\lambda = (2\pi a/\lambda)^n$ for $\lambda > 2\pi a$, where n is the emissivity index, and $Q_\lambda = 1$ for $\lambda < 2\pi a$. In a thermal fluctuation model, T is a function of time t, with T rising abruptly to a maximum temperature $T_{\max}$ when a UV photon of energy $E_{\rm ph}$ is absorbed, and then decreasing as the grain radiatively cools. Thus, the time average of P_λ is

$$\bar{P}_\lambda = \int \pi B_\lambda[T(t)] 4\pi a^2 Q_\lambda(a) R_{\rm ph}\, dt , \tag{A2}$$

where $R_{\rm ph}$ is the rate of absorption of UV photons. For simplicity, the UV photon energy is fixed. The value of $R_{\rm ph}$ is given by $R_{\rm ph} = F_{\rm UV} Q_{\rm UV}(a) \pi a^2$, where $F_{\rm UV}$ is the flux of UV photons incident on the grain and $Q_{\rm UV}(a)$ equals $Q_\lambda(a)$ at the wavelength $\lambda_{\rm UV}$ of the UV photons. Due to the small grain sizes required for the thermal fluctuation model, $Q_{\rm UV} = (2\pi a/\lambda_{\rm UV})^n$ even at UV wavelengths (Paper II).

The only part of the integrand in equation (A2) depending on t is $B_\lambda(T)$. To find $\int B_\lambda(T) dt$, one notes that

$$\int B_\lambda(T) dt = \int B_\lambda(T)(dt/dT) dT = \int B_\lambda(T)(dt/dE)(dE/dT) dT , \tag{A3}$$

where dE/dt is the rate of radiative energy loss and dE/dT is the heat capacity C_V of the grain. At the temperatures of interest, $C_V = 3Nk$, where $3N$ is the number of degrees of freedom in the grain. The value of N is $\sim(a/d)^3$, where d is the distance between atoms or molecules in the grain (Paper II). The cooling rate is

$$dE/dt = \int P_\lambda\, d\lambda = \int \pi B_\lambda(T) 4\pi a^2 Q_\lambda(a) d\lambda = 4\pi a^{2+n} Q_n \sigma T^{4+n} , \tag{A4}$$

where σ is the Stefan-Boltzmann constant and Q_n is a constant depending on n. The Planck function $B_\lambda(T) = 2hc^2\lambda^{-5}(e^x - 1)^{-1}$, where $x = hc/\lambda kT$. Thus,

$$\int B_\lambda(T) dt = \int 2hc^2\lambda^{-5}(e^x - 1)^{-1}(4\pi a^{2+n} Q_n \sigma T^{4+n})^{-1} 3Nk dT . \tag{A5}$$

Rewriting this integral in terms of x gives

$$\int B_\lambda(T) dt = K_1 a^{1-n} \lambda^{n-2} \int x^{2+n}(e^x - 1)^{-1} dx , \tag{A6}$$

where $K_1 = (3ck^{4+n})/[2\pi Q_n \sigma d^3 (hc)^{2+n}]$. The integration limits in equation (A6) in terms of T are the highest temperature reached by the grain, T_{max}, and the lowest temperature reached by the grain before absorbing another photon, which is close to 0; this corresponds to integration limits in x of x_{max} and infinity, where $x_{max} = hc/\lambda k T_{max}$. For simplicity, $I_1(x_{max})$ is defined to be $\int x^{2+n}(e^x - 1)^{-1} dx$. Thus, the final expression for the time-averaged power per unit wavelength is

$$\bar{P}_\lambda = 4\pi^2 a^2 (2\pi a/\lambda)^n F_{UV} (2\pi a/\lambda_{UV})^n \pi a^2 K_1 a^{1-n} \lambda^{n-2} I_1(x_{max}) = K_2 \lambda^{-2} a^{5+n} I_1(x_{max}) , \quad \text{(A7)}$$

where $K_2 = 4\pi^3 K_1 F_{UV} (2\pi)^{2n} \lambda_{UV}^{-n}$.

The next step in determining the wavelength dependence of the reflection nebula emission is to find $\langle \bar{P}_\lambda \rangle$, the value of $\bar{P}_\lambda$ integrated over a grain size distribution $n(a)da$. The grain size distribution of Mathis, Rumpl, and Nordsieck (1977), $n(a)da = n_0 a^p da$ with $p = -3.5$, is adopted. Thus,

$$\langle \bar{P}_\lambda \rangle = \int \bar{P}_\lambda n(a) da = \int K_2 \lambda^{-2} a^{5+n} I_1(x_{max}) n_0 a^p da . \quad \text{(A8)}$$

The value of a is related to x_{max} through T_{max}, since $E_{ph} = \int C_V(T) dT = 3NkT_{max} = 3a^3 k T_{max}/d^3$. Rewriting the integral in equation (A8) in terms of x_{max}, one finds

$$\langle \bar{P}_\lambda \rangle = K_3 \lambda^\beta \int x_{max}^{1+\beta} I_1(x_{max}) dx_{max} , \quad \text{(A9)}$$

where $K_3 = K_2 (n_0/3)(E_{ph} d^3/3hc)^{2+\beta}$, and $\beta = (n + p)/3$. The integration limits in equation (A9), expressed in terms of T_{max}, were chosen to be approximately the grain sublimation temperature, $T_{max} \approx 2000$ K, and the grain temperature at which the contribution to the longest wavelength emission observed begins to be negligible, or $T_{max} \approx 100$ K. Since x_{max} depends on λ, the integral over x_{max} (eq. [A9]) must be evaluated numerically to determine how $\langle \bar{P}_\lambda \rangle$ depends on λ.

The results for $n = 2$ are shown in Figure 2. The solid curve is the prediction of the thermal fluctuation model for the spectral dependence of the continuum emission, arbitrarily normalized to the observations at 10.75 μm in NGC 7023 and to the upper limit at 11.74 μm in NGC 2023, while the points are the data for NGC 7023 and NGC 2023 from Figure 1. The shape of the solid curve is insensitive to the value of the grain index n adopted, as well as to the grain size index p and to the lowest value of T_{max} chosen. The curve agrees reasonably well with the observations at longer wavelengths and falls short at the shorter wavelengths, as might be expected from the observed increase in the fraction of the emission due to reflected light at shorter wavelengths (Sellgren, Werner, and Dinerstein 1985). The agreement at the shortest wavelengths is sensitive to the largest value of T_{max} chosen, an effect that will be explored in more detail in Sellgren, Werner, and Dinerstein (1985).

The above calculation neglects the effects of the unidentified features on the cooling of the grains. We chose to exclude this effect since the features and continuum may be emitted by different grains. It is estimated that including this additional cooling would have little effect on the predicted shape of the continuum. Each feature contributes significantly to the grain cooling only at temperatures whose Planck functions peak near the feature wavelength. The maximum contribution of the 3.3 and 11.3 μm features is 10%–20%; the maximum contribution of the 6.2 and 7.7 μm features can be either somewhat less or somewhat more, depending on what continuum level is adopted. Because the features are fairly evenly distributed throughout the 3–11 μm region, this additional cooling is unlikely to significantly alter the predicted shape or slope of the near-infrared continuum.

REFERENCES

Aannestad, P. A., and Kenyon, S. J. 1979, *Ap. J.*, **230**, 771.
Aitken, D. K. 1981, in *IAU Symposium 96, Infrared Astronomy*, ed. C. G. Wynn-Williams, and D. P. Cruikshank (Dordrecht: Reidel), p. 214.
Allamandola, L. J., Greenberg, J. M., and Norman, C. A. 1979, *Astr. Ap.*, **77**, 66.
Allamandola, L. J., Tielens, A. G. G. M., and Barker, J. R. 1985*a*, *Ap. J. (Letters)*, **290**, L25.
———. 1985*b*, in preparation.
Allen, M., and Robinson, G. W. 1975, *Ap. J.*, **195**, 81.
Beckwith, S., Evans, N. J., Becklin, E. E., and Neugebauer, G. 1976, *Ap. J.*, **208**, 390.
Draine, B. T., and Anderson, N. 1985, *Ap. J.*, **292**, 494.
Duley, W. W. 1973, *Nature Phys. Sci.*, **244**, 57.
Dwek, E., Sellgren, K., Soifer, B. T., and Werner, M. W. 1980, *Ap. J.*, **238**, 140.
Elias, J. H., Frogel, J. A., Matthews, K., and Neugebauer, G. 1982, *A.J.*, **87**, 1029.
Greenberg, J. M., and Hong, S. S. 1974, in *IAU Symposium 60, Galactic Radio Astronomy*, ed. F. Kerr and S. C. Simonson III (Dordrecht: Reidel).
Harvey, P. M., Thronson, H. A., and Gatley, I. 1980, *Ap. J.*, **235**, 894.
Harwit, M. 1975, *Ap. J.*, **199**, 398.
Leger, A., and Puget, J. L. 1984, *Astr. Ap.*, **137**, L5.
Mathis, J. S., Rumpl, W., and Nordsieck, K. H. 1977, *Ap. J.*, **217**, 425.
Phillips, M. M., Aitken, D. K., and Roche, P. F. 1985, *M.N.R.A.S.*, **207**, 25.
Price, S. D., and Walker, R. G. 1976, AFGL-TR-76-0208.
Puget, J. L., Leger, A., and Boulanger, F. 1985, *Astr. Ap.*, **142**, L19.
Purcell, E. M. 1976, *Ap. J.*, **206**, 685.
Sellgren, K. 1981, *Ap. J.*, **245**, 138.
———. 1984, *Ap. J.*, **277**, 623 (Paper II).
Sellgren, K., Werner, M. W., and Dinerstein, H. L. 1983, *Ap. J. (Letters)*, **271**, L13 (Paper I).
———. 1985, in preparation.
Whitcomb, S. E., Gatley, I., Hildebrand, R. H., Keene, J., Sellgren, K., and Werner, M. W. 1981, *Ap. J.*, **246**, 416.
Witteborn, F. C., and Bregman, J. D. 1984, preprint.

L. J. ALLAMANDOLA, J. D. BREGMAN, M. W. WERNER, and D. H. WOODEN: M/S 245-6, NASA Ames Research Center, Moffett Field, CA 94035

K. SELLGREN: Institute for Astronomy, 2680 Woodlawn Drive, Honolulu, HI 96822